Chem Soc Rev

TUTORIAL REVIEW

Properties- and applications of quasicrystals and complex metallic alloys†

Jean-Marie Dubois*

This article aims at an account of what is known about the potential for applications of quasicrystals and related compounds, the so-called family of Complex Metallic Alloys (CMAs‡). Attention is focused at aluminium-based CMAs, which comprise a large number of crystalline compounds and quasicrystals made of aluminium alloyed with transition metals (like Fe or Cu) or normal metals like Mg. Depending on composition, the structural complexity varies from a few atoms per unit cell up to thousands of atoms. Quasicrystals appear then as CMAs of ultimate complexity and exhibit a lattice that shows no periodicity anymore in the usual 3-dimensional space. Properties change dramatically with lattice complexity and turn the metal-type behaviour of simple Al-based crystals into a far more complex behaviour, with a fingerprint of semiconductors that may be exploited in various applications, potential or realised. An account of the ones known to the author is given in the light of the relevant properties, namely light absorption, reduced adhesion and friction, heat insulation, reinforcement of composites for mechanical devices, and few more exotic ones. The role played by the search for applications of quasicrystals in the development of the field is briefly addressed in the concluding section.

A Introduction

Danny Shechtman discovered quasicrystals in melt-spun ribbons of an Al–Mn alloy thirty years ago.[1] Last year, he was awarded the Nobel Prize in Chemistry because his outstanding discovery forced the scientific community to change the way solid condensed matter was understood until then. The objective of this article is not to deal with the historical background of the discovery, nor is it to explain the fundamental issues associated with it in mathematics, crystallography, arts, *etc.* This is the subject of the other articles in this special issue that the reader should have read before the present article. The aim of this review is to describe the main physical properties that quasicrystals inherit from the absence of periodicity, and to introduce the few applications foreseen so far for those materials.

Very few years after the initial discovery of the Al₄Mn quasicrystal by Shechtman *et al.*,[1] Tsai pointed out during his PhD work at Tohoku University, Japan, the formation of several stable icosahedral[2] and decagonal[3] quasicrystals§ in

Born in 1950, Jean-Marie Dubois is a Distinguished Director of Research at CNRS, France, and the head of a 400-staff public research institute working in the field of materials science and engineering. He has authored 330 scientific articles, 14 patents, and 7 books. After establishing structure models for metallic glasses and quasicrystals, Dubois became interested in applied properties of these materials: heat insulation, low adhesive properties and

Jean-Marie Dubois

infrared light absorption, cold-welding and solid–solid adhesion under vacuum of complex metallic alloys (CMAs) against steel. More generally, he studies the interplay between structure complexity and physical properties of CMAs.

Institut Jean Lamour (UMR 7198 INC-CNRS – Université de Lorraine), Ecole des Mines, Parc de Saurupt, CS14234, 54042 Nancy, France. E-mail: jean-marie.dubois@ijl.nancy-universite.fr; Tel: +33 383584274

† Part of a themed issue on Quasicrystals in honour of the 2011 Nobel Prize in Chemistry winner, Professor Dan Shechtman.
‡ The acronym CMA, for Complex Metallic Alloys, was designed by K. Urban (Peter Grünberg Institute, Juelich) and the present author to define both a specific family of alloys, and the European Network of Excellence that has supported research about this topic in Europe until 2010.

§ We assume that the reader is familiar with these terms after reading the other articles in this special issue. Also, space is too short to introduce any historical background of the discovery of quasicrystals that has no direct relevance to the present review. Better information may be found elsewhere in this issue of Chemical Society Reviews, or in ref. 8.

ternary Al-based intermetallic systems containing Fe and Cu, or Pd and Mn, or Ni and Co. He had identified the Al–Cu–Fe system as a potential candidate for the growth of a quasicrystal upon reading an early work published before World War II.[4] During the two decades that followed, few more stable quasicrystals were discovered, based on a major constituent different from aluminium. This was the case *e.g.* of the stable, binary Cd–Ca icosahedral compound, also discovered by Tsai's group.[5] Of this series of new quasicrystals, none was studied from the standpoint of its potential applications, with the exception yet of the Ti–Ni–Zr system that shows potential for hydrogen storage.[6] The Al–Li–Cu system, the first alloy that was shown to yield a stable quasicrystal,[7] was searched for reducing the weight of aeronautical alloys. To the best of the author's knowledge, it has not been converted into a practical product.

It is therefore the Al–TM (TM = transition metals like Fe, Cu, or Pd, Mn, or Co, Ni, or Cu, Ni, *etc.*) systems that show today the best potential for practical usefulness.[8] Applications realised so far, or envisaged, encompass different categories, depending on the type of property they shall exploit:

(a) transport properties: infra-red absorption for heating devices, reduced adhesion and friction for surface functions, heat insulation, and data storage based on contactless thermal cells

(b) mechanical reinforcement by precipitates grown *in situ*, or addition of reinforcement particles in metal or polymer matrices

(c) chemical properties for the sake of producing corrosion resistant surfaces, low cost catalysts or hydrogen storage media.

Although the list of such possible applications cannot be completed at a given time, the article will trace the most well known ones and place them in the light of our knowledge of the supporting property. Attention will be placed first on the correlation between composition and structure complexity in the family of Al–TM compounds. In a second step, we will observe how electron transport properties vary with the complexity of the underlying lattice. To this end, we will assess the degree of complexity of the lattice using a very simple and straightforward complexity index called β_C. Owing to the extreme importance of processing a metallurgical product in view of a certain application, few lines will then be dedicated to the various metallurgical routes used so far to prepare quasicrystals and related alloys either in bulk form, as single crystals, or as surface coatings and thin films. With these preliminary data in mind, we will thus be able to explore the potential of applications of those alloys and compounds, following the list given above in three different categories. The conclusion section will insist on the prominent role played by the potential applications of these materials in the development of the field and its attraction towards a large number of scientists aside the communities of crystallographers and mathematicians.

A1 Aluminium-based complex intermetallics and quasicrystals

Fig. 1 presents a standard cut at $T = 700\ °C$ through an up-to-date version of the isothermal Al–Cu–Fe phase diagram.[9] Several compounds are labelled with Greek letters in this diagram among which are well known binaries (like θ-Al$_2$Cu)
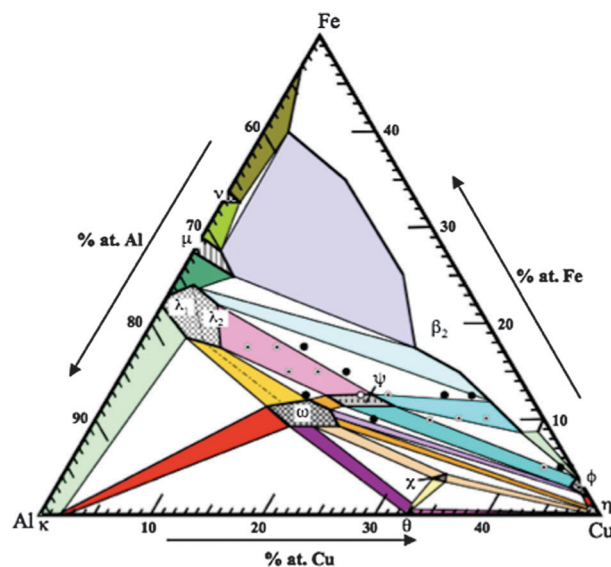

Fig. 1 Isothermal section at $T = 700\ °C$ through the Al-rich corner of the Al–Cu–Fe phase diagram. Greek letters label binary and ternary compounds. The approximants associated with the icosahedral compound (Ψ-phase) are located within the same region of the phase diagram. Redrawn after ref. 9.

or pseudo-binaries (like φ-Al$_{10}$Cu$_{10}$Fe). Space is too short in this review to describe them all, but more information may easily be found in standard crystal structure handbooks. Near the centre of the Al-rich corner of the diagram shown in Fig. 1 is the ψ-phase, or icosahedral phase, discovered by Tsai. The stability range of this phase is rather narrow; it shrinks to an even smaller area when the temperature decreases down to room temperature. Furthermore, the region in the phase diagram in the near vicinity of this area also contains approximant crystals with nearly identical composition and very similar atomic order as the quasicrystal.[10] Approximants are compounds with a periodic lattice that are very close to a parent quasicrystal (a) because they can be referred to the same high dimensional periodic lattice, but according to a projection scheme ruled by rational numbers approximating the golden mean $\tau = (1 + \sqrt{5})/2 \approx 1.618...$ and (b) because they depart from the quasicrystal composition only by small amounts. Depending on the approximation number, which will be equal to the ratio between two successive members of the Fibonacci series 1/1, 3/2, 5/3, *etc.*, the size of the unit cell will contain more and more atoms and be characterized by increasingly large lattice parameters (more information may be found by the interested reader in classical text books like ref. 11). An important point to mention already at this stage is the fact that only the first members in the series were found so far.[10,12] The largest unit cell size discovered experimentally corresponds to the Al$_{60.3}$Cu$_{30.9}$Fe$_{9.7}$ compound,¶ with lattice parameters $a = 3.21$ nm; $b = 11.63$ nm; $c = 1.98$ nm, *i.e.* nearly 5000 atoms per unit cell.

Interestingly, periodic stacks of alternating flat and puckered periodic layers of atoms may be found as well. They mimic the

---

¶ All compositions are given either in at% or in numbers of atoms per molecular unit throughout the article.
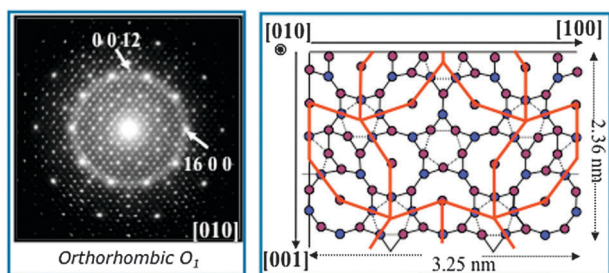
Fig. 2 Views of the reciprocal space (left) and real space (right) of one of the orthorhombic compounds representative of complex intermetallics that form in the Al–Fe(–Cu)–Cr system. Only part of the atoms in the layer stacked perpendicular to the pseudo-ten-fold axis shown in the right part of the figure is drawn to simplify the figure.

decagonal quasicrystal when they show decagonal rotational symmetry perpendicular to the stack axis. A famous example is the λ-$Al_{13}(Fe,Cu)_4$ compound that is visible in the left side part of Fig. 1. Except for the bcc B2-CsCl-type phase, solubility of the third element is usually small, or corresponds to a well-defined stoichiometry like in the ω-Al_7Cu_2Fe compound or the quasicrystal already introduced, which has a slightly different stoichiometry. Addition of a fourth element like Cr or Mn leads to an essentially different phase map, in which examples of highly complex compounds may be found as approximants of the decagonal phase.[13] Fig. 2 presents an example of a large unit cell size orthorhombic compound, both in reciprocal space (left side of the figure) and in real space (right) that is characteristic of the Al–Fe(–Cu)–Cr system. The pseudo-ten-fold symmetry is clearly visible in reciprocal space. Only part of the atoms is drawn in real space, for the sake of clarity of the figure. Decagonal rings and pentagonal motifs are easy to identify. The periodic stacking is perpendicular to that of the figure. It leads to a parameter $c = 1.24$ nm, identical to the one of the decagonal phase of similar composition. Shorter, and even longer stack periods are known in different systems.

Similarly, the Al–Pd–Mn phase diagram shows a broad variety of compounds, ranging from the simple B2-CsCl-type phase to highly complex crystals exhibiting large to huge unit cells, or a quasicrystal.[14] In the following, we will make use of experimental data acquired using a series of compounds that belong to such alloy systems. Most often, these will be binary or ternary compounds, but in few occasions we will also refer to quaternary compounds of the Al–Cu–Fe–Cr system like the one illustrated in Fig. 2. The preparation steps of those samples will be briefly evocated in Section C hereafter. Characterization of the crystal structures is beyond the scope of this review, but may be found elsewhere.[8]

A2 Structure complexity

Complexity of a crystal compound is difficult to assess and is often understood as the difficulty to describe it in its fine details. An example was already shown in Fig. 2, which emphasises the high density of spots, including close to the origin, that populate the reciprocal space of this compound. Another equivalent mirror of complexity is the number of facets found on the successive Brillouin zones of the crystal. The Jones zone, which is the Brillouin zone constructed using

the most intense diffraction peaks, however, does not necessarily correspond to a highly facetted polyhedron. The Jones zone plays a very important role in the stability and transport properties of CMAs, as we will see in the next section. Therefore, we prefer to refer complexity to an as simple as possible indicator, keeping in mind that more appropriate or more efficient ones may be found to place a given property on a rational scale.

As far as transport properties of Al-based CMAs are concerned, we attach a simple index to the complexity of the unit cell:

$$\beta_C = \text{Ln}(N_{UC}) \qquad (1)$$

where N_{UC} is the number of atoms in the unit cell of the crystal. The complexity index takes values between $\beta_C = \text{Ln}(2)$ for bcc lattices and Ln(few thousands) for the most complex periodic CMAs known so far. We avoid undesirable infinite numbers by noticing that an icosahedral grain is never of infinite size, although no unit cell may be defined in 3D space. If the sample is an atom gram of matter, then $\beta_C = \text{Ln}(N)$ with N being Avogadro's number, which is a finite number $\text{Ln}(N) \approx 54$. It is worth noticing that, within a constant factor, β_C is equal to the Shannon entropy of the unit cell of a single-constituent crystal at 0 K.

The complexity index can be extended to encompass as well complexity of periodic stacks of aperiodic layers. For the decagonal phase (or for the pentagonal approximant), it reads:

$$\beta_C(\text{deca}) = \text{Ln}(m_z) + 2/3\beta_C(\text{ico}) \qquad (2)$$

where $\beta_C(\text{ico})$ is the complexity index defined by eqn (1) for the icosahedral phase and m_z is the number of puckered layers stacked along the periodic axis of the deca-phase (the Al–Cu–Co decagonal phase has $m_z = 6$ such layers, hence a period along the 10-fold axis of $c = 1.24$ nm whereas the Al–Ni–Co phase has a shorter period of $c = 4.1$ nm with $m_z = 2$ only). Similarly, for one-dimensional aperiodic crystals, we have:

$$\beta_C(1D) = \text{Ln}(m_x) + \text{Ln}(m_y) + 1/3\beta_C(\text{ico})$$

with m_x and m_y being the numbers of stacks along the two periodic directions of the crystal. In the following, we will refer to the complexity of each individual compound by using simply its β_C index and we will drop all un-necessary labels like ico or deca.

B   Overview on electron transport properties of complex metallic alloys

B1 Hybridization, Brillouin zone and Fermi surface interactions

Early after the discovery of quasicrystals, it was realized that they obey the same stability rules as many other crystalline intermetallics like the Cu–Zn γ-brass phase.[15] Those rules are known under the name of Hume-Rothery[16] who was the first to understand that specific binary compounds, which show a weak difference in the constituents sizes and an appropriate electron to atom (e⁻/at) ratio, are selected because they

produce a matching between the Fermi surface and the Brillouin zone characteristic of that structure. When this mechanism takes place, a gap opens along the direction in reciprocal space where the Fermi surface touches a facet of the Brillouin zone, thus leading to an increased density of states below the Fermi energy (E_F), or equivalently an increased stability of this specific crystal structure. Application of this principle to quasicrystals is not straightforward however. First, a true Brillouin zone does not exist and one has to refer to the Jones zone instead, assuming that the scattering potential which applies to diffraction also applies to electrons at the Fermi edge in the crystal. Second, the contribution of transition metal atoms to the valence band is ill-defined and one is forced to admit that transition elements like Fe or Mn exhibit negative valences, which need to be consistently fitted to observe a coherent trend of the stability zones for the various quasicrystals. Within this scheme, taking a valence electron contribution of Fe equal to $V_{Fe} = -2.6$ e$^-$/at, for manganese $V_{Mn} = -2$ e$^-$/at, and logical values of $V_{Al} = +3$ e$^-$/at, $V_{Cu} = +1$ e$^-$/at, $V_{Pd} = 0$ e$^-$/at, it is observed that both Al–Cu–Fe and Al–Pd–Mn icosahedral quasicrystals form within a narrow electron concentration range around 1.8–1.9 e$^-$/at.[8] The electron concentration is simply calculated from composition $Al_xTM1_yTM2_z$ ($x + y + z = 1$) by:

$$e^-/\text{at} = xV_{Al} + yV_{TM1} + zV_{TM2} \qquad (3)$$

where TM1 and TM2 stand for two transition metals like Fe and Cu, or Mn and Pd. Al-based quasicrystals, which contain no (or little) transition metal, but only normal metals are found slightly apart from this range, but again in a narrow range around 2.1–2.2 e$^-$/at (an example is the Al–Li–Cu quasicrystal already mentioned).

Mizutani[17] has developed since a far deeper understanding of the Hume-Rothery rules for intermetallics in general, yet with emphasis on γ-brass phases and related compounds by starting from *ab initio* computations of the density of states. When doing so, he eliminated the awkward negative valences, and provided a broad, consistent scheme of the formation range of binary CMAs. Also, after several theoretical works produced in the 1990s,[18] he showed new evidence that Fermi surface–Jones zone interactions taken alone cannot explain the appearance of many stable binary intermetallics, but that hybridization effects must be considered as well. We illustrate the case with the example of the β-Al_3Mg_2 compound, which is one of the most complex compounds studied so far, with 1168 atoms per unit cell.[19] This compound, in contrast to *e.g.* the $Al_{11}Mn_4$ crystal (Fig. 3), obviously shows little contact between its Fermi surface and Jones zone (Fig. 4). In the former case, the diameter of the Fermi surface, $2k_F = 30.5$ nm^{-1}, matches perfectly the position of the sharp diffraction peaks (Fig. 3), which ensures an optimal contact of the Fermi sphere with the facets of the Jones zone, whereas in the latter case, we have $2k_F = 31.6$ nm^{-1}, which falls well above the position of the sharp diffraction peaks (Fig. 4). As a consequence, the Fermi sphere overlaps the Jones zone.

As a matter of fact, a sharp peak of d-like states forms in the Al and Mg 3s,d partial densities of states (DOSs) just under E_F (Fig. 5). The narrow width of these two peaks identifies them
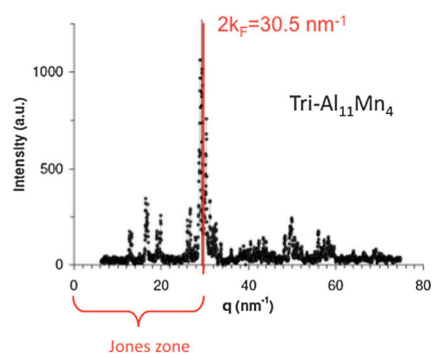

Fig. 3 Diffraction pattern (intensity *versus* momentum transfer; λ = Kα₁ Co) characteristic of the $Al_{11}Mn_4$ Hume-Rothery compound. The diameter of the Fermi sphere matches perfectly the position of the sharp diffraction peaks that define the Jones zones.

clearly as arising from localised, or equivalently d-states, although the pure constituents, Al and Mg, do not show d-states below their respective Fermi levels. Further analysis of the data points out a hybridization effect between the Al3p and Al3s,d states and, when the Mg edge is studied, Mg3p and 3s,d states.[20] The mechanism is the same as the one illustrated
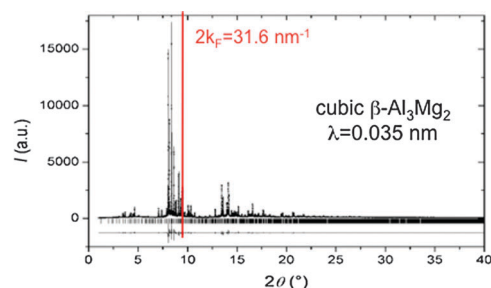
Fig. 4 Diffraction pattern (intensity *versus* twice the Bragg angle θ) of the β-Al_3Mg_2 compound. Observe how the Fermi sphere overlaps the Jones zone. Redrawn from ref. 19.
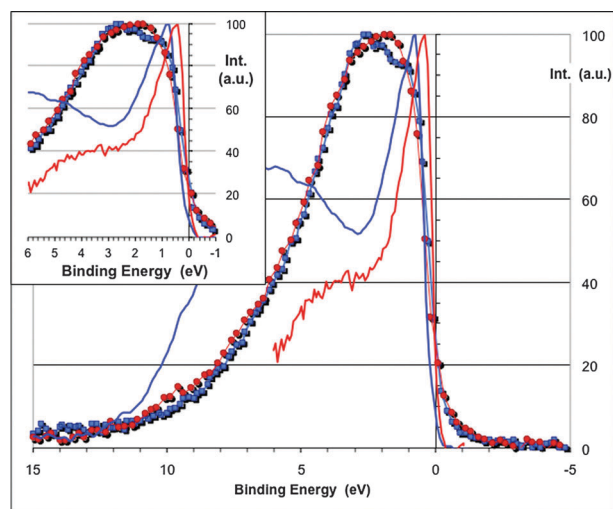
Fig. 5 Partial densities of Al3s,d (blue solid line), Mg3s,d (red solid line), Al3p (blue dotted thin line) and Mg3p (red dotted thin line) states as supplied by XES experiments.[20] A blow up of the energy scale near the Fermi energy set to 0 binding energy is given in the inset.
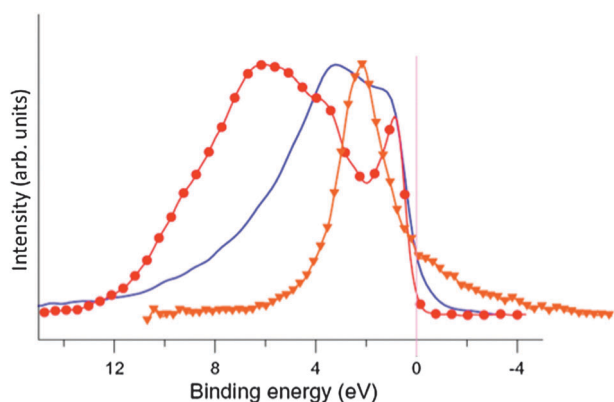
Fig. 6 Partial densities of states derived from XES experiments on the Al_3Ni compound.[20] The thin solid line represents the Al3p states, the dotted line, the Al3s,d states and the line marked with triangles, the Ni3d states. The Fermi energy is set to 0 binding energy.

in Fig. 6 for the case of the orthorhombic Al_3Ni compound, which has the well-known Fe_3C cementite structure. The data shown in Fig. 6 are based upon a soft X-ray emission spectroscopy (XES) study,[21] which provides separately partial densities of states for the different constituent species, namely here Al3p, Al3s,d and Ni3d states.[20] The partial Ni3d DOS appears as a rather narrow peak, under E_F for this compound, or overlapping it in other compounds of Al alloyed to a transition metal of the middle of the 3d series. A clear interaction, or hybridization, is seen between the 3d states and the Al3p and Al3s,d states that are split into bonding and antibonding states, thus enhancing the stability of the system. It is a similar, yet less marked, mechanism that applies in β-Al_3Mg_2 (Fig. 5), since (i) a shoulder forms on the Al3p DOS, which corresponds on the binding energy scale to the maximum of the Al3s,d DOS, whereas (ii) the maximum of the Mg3p DOS is shifted to higher binding energies due to a repulsion from the maximum of the Mg3s,d DOS. The two effects combine to stabilize the giant unit cell of the β-Al_3Mg_2. Unfortunately, *ab initio* computation of the electronic structure is beyond the performance of current computers for so many atoms in the unit cell and it is not feasible yet to obtain better insight into the DOS of this compound.

B2 Partial density of Al3p states

The total DOS at the Fermi energy ($N(E_F)$) is key to interpret the electron transport properties of metallic alloys and compounds. For CMAs and quasicrystals of large unit cell, it was shown by Mizutani,[22] that transport occurs *via* a hopping mechanism similar to the one imagined by Mott for disordered materials.[23] In this case, Mizutani predicts that conductivity should scale as the square of $N(E_F)$, which is indeed verified experimentally.[22] The same conclusion is valid for the partial Al3p DOS at E_F, which we label $n(E_F)$ in this article.[24] We present in Fig. 7 a summary of many data measured in a series of Al-based CMAs. The x-axis is labelled according to the electron concentration per atom introduced in eqn (3), which simplifies the presentation in the y, z concentration field. A sharp minimum of the Al3p DOS is observed for the icosahedral crystals, whereas the maximum is given by the pure fcc Al metal (in the normalized units adapted to XES, this value is
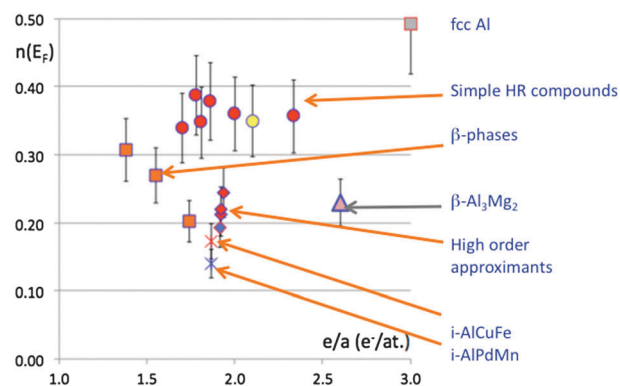

Fig. 7 Partial Al3p density of states at the Fermi energy measured in various compounds of the Al–Cu–Fe system, the β-Al_3Mg_2 (triangle) and icosahedral AlPdMn by XES. The abscissa axis is defined according to eqn (3). The grey square represents fcc Al, which by definition of XES intensity units is set to $n(E_F) = 0.5$. The orange squares on the left side of the figure are for various B2-CsCl type phases of varying composition. The dots in the central part of the figure represent different binary and ternary compounds, including the ω-Al_7Cu_2Fe compound (yellow dot). The diamonds stand for high order Al–Cu–Fe approximants (red symbols) and the pentagonal approximant (blue symbol). Quasicrystals are represented by stars.

by definition of a free electron metal equal to $n^f(E_F) = 0.5$ [21]). The other CMAs supply values of $n(E_F)$ that fall within this range, depending on the compound nature: approximants are found close, but above the value of $n(E_F)$ for the quasicrystal whereas Hume-Rothery compounds of smaller unit cell size lie around $n(E_F) = 0.3$ (in the units adapted to XES).

It is interesting to notice (Fig. 8) that the electronic resistivity ρ of large unit cell CMAs satisfies Mizutani's prediction and scales as a power 2 law of $n(E_F)$. For compounds with much smaller unit cell, this is not true anymore and the scaling is indicative of a complex transport mechanism, which cannot be simply ballistic, or proportional to the DOS at E_F (Fig. 8).

B3 Self-organised criticality of transport properties in Al-based CMAs

The size of the unit cell seems thus to have direct relationship to electronic transport properties of CMAs. We will focus here on two properties, namely electron transport itself, as it can be
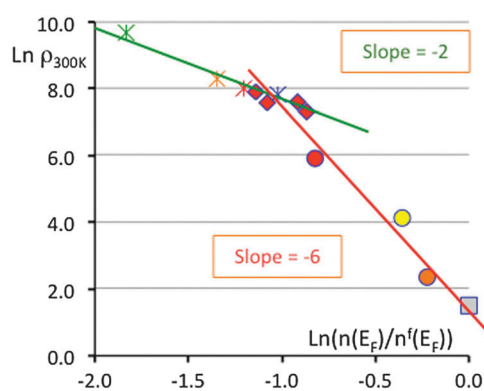
Fig. 8 Ln–Ln presentation of the room temperature resistivity of a variety of Al–Cu–Fe CMAs as a function of their partial Al3p DOS at the Fermi energy (see text). Symbols are defined as in Fig. 7.

6764 | *Chem. Soc. Rev.*, 2012, **41**, 6760–6777

This journal is © The Royal Society of Chemistry 2012

measured by a standard four-electrode method as a function of temperature, and heat diffusivity. Heat diffusivity is defined according to the Fourier equation of heat as:

$$\alpha = \kappa/\rho_{m}C_{P}$$

where κ is the thermal conductivity of the sample, ρ_{m} its specific mass and C_{P} its specific heat at constant pressure. In all CMAs studied in this article, room temperature is close to Debye temperature and therefore C_{P} is close to the Dulong–Petit limit ($C_{P} = 3R$). We may therefore assume a first approximation that the contribution of phonons to the transport of heat has saturated and that further variations of κ are essentially dominated by the contribution of conduction electrons. Therefore:

$$\alpha(RT) \propto \sigma(RT) = \rho^{-1}(RT)$$

where $\sigma(RT)$ denotes the electronic conductivity at room temperature and $\alpha(RT)$ is the heat diffusivity, also measured at room temperature RT. The two properties, however, are measured using totally different samples, of different shapes and volumes, by independent methods. Dolinsek et al.[25] and Dubois and his co-workers,[26] produced data sets for the electron conductivity and heat diffusivity measurements, respectively. They are in very good agreement with other sets of measurements produced on similar samples.[27]

Fig. 9 presents the electric resistivity measured as a function of temperature in an ensemble of CMA samples that are arranged in the figure from the simplest crystal structure of
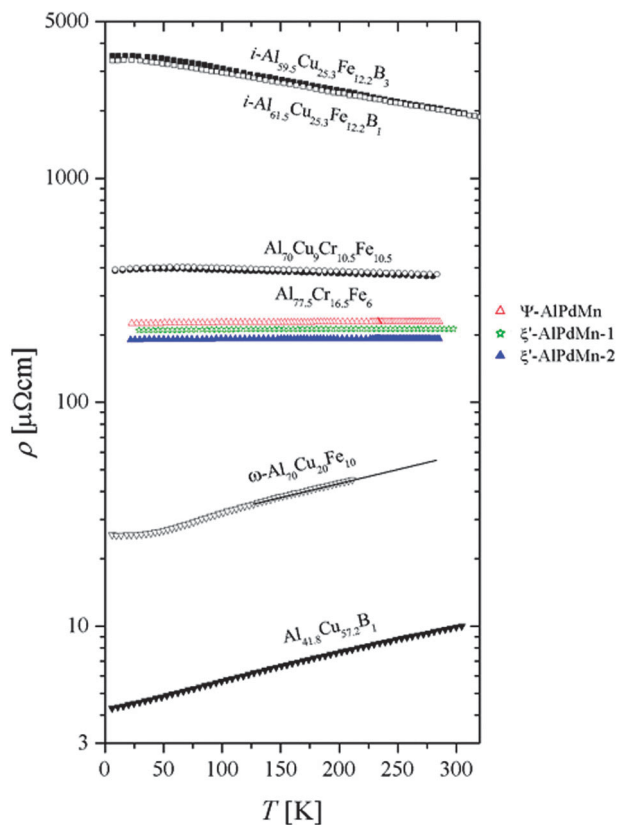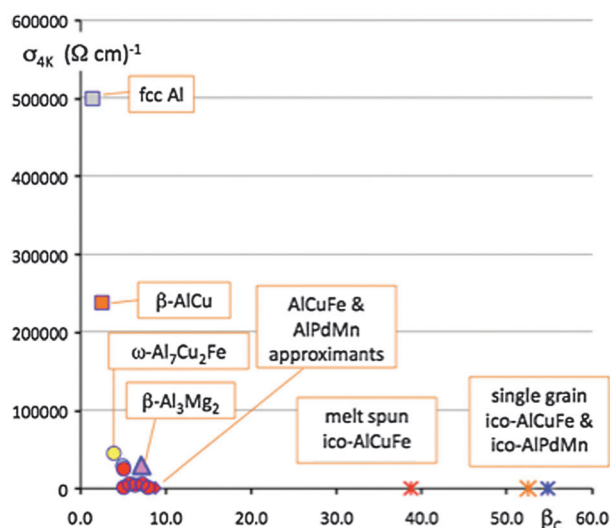

Fig. 10 Low temperature resistivity measured in various CMAs as indicated by the labels, presented as a function of the respective complexity indices of the compounds. Symbols are as in Fig. 7.

the B2-CsCl type placed at the bottom up to quasicrystals placed in the top of the figure.[25] The well known reversal of the temperature coefficient of the resistivity can be observed in the middle of the figure, for approximant crystals containing a few hundreds of atoms per unit cell, while the low temperature resistivity is clearly small for small unit cell crystals, and the largest for quasicrystals. This modification is indicative of the change of electron transport mechanism already pointed out in Fig. 8. Fig. 10 summarises how resistivity changes over a few orders of magnitude when the crystal complexity spans the range $\beta_{C} = Ln(4)$ for fcc aluminium up to β_{C} calculated according to eqn (1) for the icosahedral crystal (according, respectively, to eqn (2) for the pentagonal approximant).‖

Although samples and experimental set-up are entirely different, the same trend is observed in the heat diffusivity data (Fig. 11). A slight scatter is observed however, due to the mass effect arising from change of the nature of the TM element entering the CMA composition, yet with little effect on the number density of the compound, which is always found within a narrow range between 60 and 70 at nm^{-3}. Neglecting small variations that occur from sample to sample depending upon the specific choice of concentration and nature of the chemical constituents of the compounds, it is then appropriate to summarize all data on a Ln–Ln scale as is shown in Fig. 12 for low temperature conductivity and in Fig. 13 for heat diffusivity at room temperature (the meaning of each symbol in Fig. 12 is identified in the inset, whereas in Fig. 13 we distinguish only between specimens of smaller and larger unit cells; note that the two sets of samples are not identical). Fig. 14 presents again the very same data as in Fig. 7, but on a Ln–Ln scale of $n(E_{F})$ referred to the Al concentration in the sample versus the crystal complexity of the compounds.

The Ln–Ln presentation smears out all details and it is consistently found that $n(E_{F})$ scales as a power law of β_{C}, with exponent equal to $\frac{1}{2}$ of the scaling exponents of the

Fig. 9 Electronic resistivity as a function of temperature measured in a series of CMAs with lattice complexity increasing from the bottom of the figure to the top.[25]

‖ The computation of β_{C} for the B2-phases has to take into account the actual superstructure of each sample.
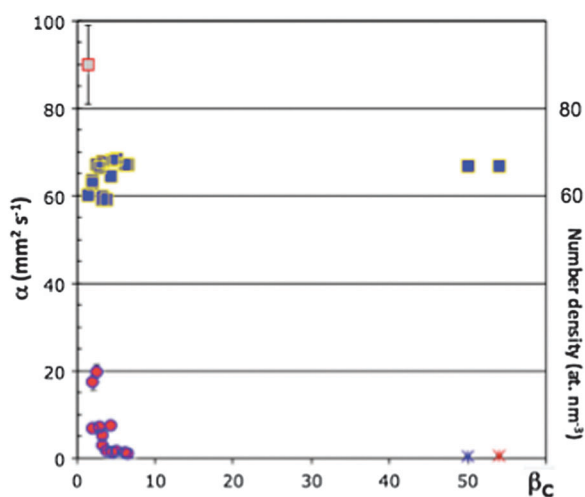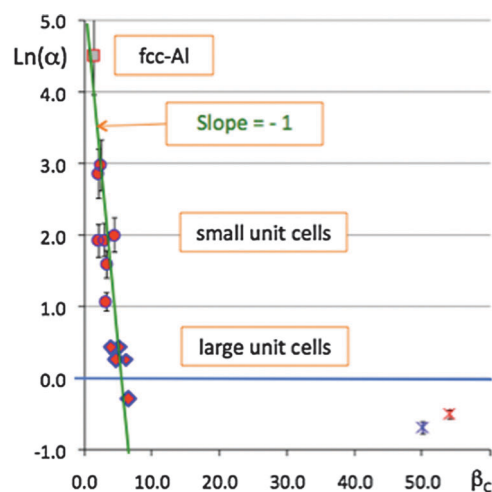
Fig. 11 Room temperature thermal diffusivity (left side y-axis) measured in several Al-TM CMAs as a function of their respective β_C index.[26] The grey square stands for fcc Al and the stars for icosahedral compounds. The number density of each compound is represented by a blue square symbol (right side y-axis).
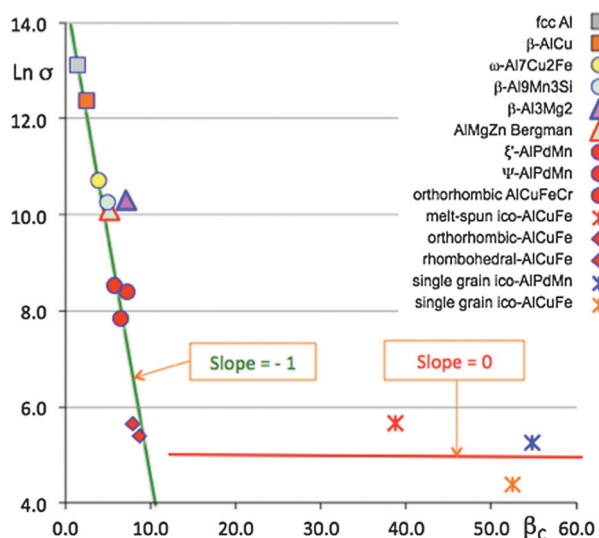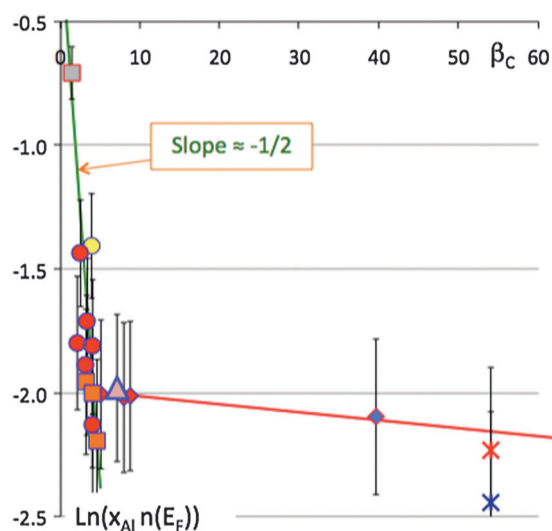

Fig. 12 Ln–Ln presentation of the same data as in Fig. 9 and 10, but converted in low temperature electronic conductivity, as a function of β_C. All CMAs, except quasicrystals, fall on the same line with slope -1. The β-Al$_3$Mg$_2$ compound is found slightly apart the line, but contains no transition metal, in contrast to all previous compounds.

electron transport properties, Fig. 12 and 13, which are both found very close to -1 within a broad range of β_C values up to about $\beta_C = 8$, i.e. a few thousands of atoms per unit cell. Compounds with much larger unit cells, namely the Al–Cu–Fe pentagonal approximant and the icosahedral crystals, do not obey the scaling law and fall aside the measure of the transport property characteristic of the periodic CMA with largest unit cell.

These findings lead us to three important conclusions at this stage. First, the Ln–Ln correlations shown in Fig. 12 and 13 are very much reminiscent of self-organised criticality (SOC) as was first pointed out by Bak for totally different systems like sand pile avalanches or earthquakes.[28] In all such examples, the frequency with which a certain phenomenon of magnitude m

Fig. 13 Same presentation as in Fig. 12, but for the room temperature heat diffusivity already shown in Fig. 11.

Fig. 14 Ln–Ln presentation of the partial Al3p DOS referred to the actual Al concentration in the compound versus its complexity. The symbols have the same meaning as in Fig. 7. Knowing Fig. 8 and 12, the observed $-1/2$ slope is consistent with Mizutani's theory.

occurs scales as a power law m^a, with $a \approx -1$, magnitude being understood either as the Richter magnitude for earthquakes, or size of an avalanche for a sand pile. In CMAs, the hopping mechanism that drives the conductivity should therefore scale also as a power law of the space offered in the crystal for it to preserve coherence. Yet, the theoretical meaning hidden behind the experimental evidence provided in those figures lies beyond the scope of the present review.

Second, and consistent with the previous conclusion, it is surprising to see that no periodic crystal is found experimentally, in spite now of years of research, beyond a certain value of β_C located around $\beta_C = 8$. The one-dimensional sizes of the unit cell become then significantly larger than the electron mean free path. Coherence between adjacent unit cells is thus no longer meaningful and Bloch's theorem of no help. Arguing that β_C is not a relevant parameter anymore, which might be true, does not add much: there is a clear gap between the upper size of periodic

CMAs observed so far and the known quasicrystals, which to the best of author's knowledge, remains un-explained. The theoretical meaning of this point is key to understand why Nature drops out periodic phases and favours instead aperiodicity for a specific composition and electronic structure. It goes beyond the simplistic Hume-Rothery approach introduced above, which cannot distinguish between periodic crystals of high complexity index, equal *e.g.* to 8, and a quasicrystal.

Third, and central to the purpose of the present review, there is a gap indeed, but transport properties do not vary much from periodic crystals of large β_C and quasicrystals. A certain range of compositions therefore exists that allows the preparation of different compounds, of different compositions, which nevertheless offer almost identical properties. This is an essential pre-requisite for the success of the synthesis of any metallurgical product, which was exploited already in the early patents of the field.[29]

## C The preparation routes of quasicrystals and complex metallic alloys

C1 Bulk materials

Bulk CMA specimens can be prepared, including in very large quantities (Fig. 15), by standard metallurgical processing: fusion of the constituents, homogenization of the liquid, solidification. Care must be taken of course to avoid pollution of the liquid by reaction with oxygen and nitrogen,[30] and more importantly to produce the final material in its stable state. Solidification of the liquid takes place indeed through a peritectic reaction, which requires transport of atoms through a solid phase and is a slow process. Usually, a thermal treatment is applied post-solidification to achieve this stable state. For Al–Cu–Fe compounds, annealing above 700 °C is often required.[31]

A straightforward way to perform the annealing and in the meantime, to shape pore-free cylindrical specimens adapted to several experiments like mechanical testing or reflectometry,

Fig. 15 Photograph of an Al–Cu–Fe–Cr ingot (weight: 1.16 kg) produced in large quantities to prepare atomized powders for plasma spray of approximant coatings on frying pans. The capability was set to 1000 kg per day.[31]
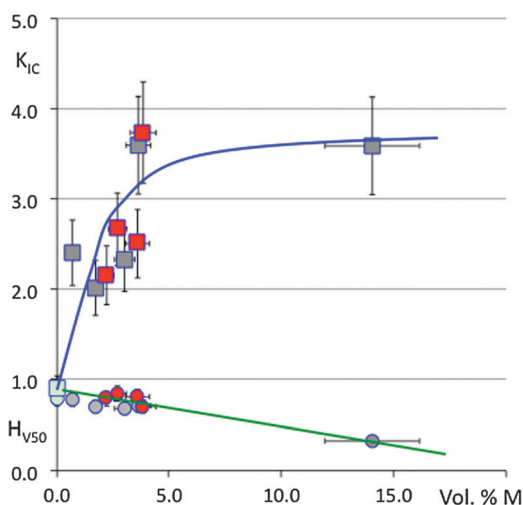
Fig. 16 Modification of the Vickers hardness (load 0.5 N, bottom part, in GPa) and toughness (deduced from Palmqvist crack lengths, top, in MPa m$^{1/2}$) upon introducing a certain volume fraction of metal M = Bi (red symbols) or Sn (grey symbols) in composites prepared by sintering under uni-axial pressure blends of icosahedral $Al_{59}Cu_{25}Fe_{12}B_3$ and M. The lines serve only to guide the eyes.

is to sinter a powder prepared from a crushed pre-alloyed ingot. Several techniques exist to do so, for instance uniaxial sintering, which we used thoroughly for many samples reported on in this review, or isostatic sintering or even spark plasma sintering. Powdering of the start ingot may be conveniently achieved by a mechanical alloying step that furthermore allows addition of new elements. This technique was used to prepare mixtures of an Al–Cu–Fe icosahedral compound with Sn or Bi additions that are immiscible in this alloy and form tiny regions located at the boundary of the grains of the former alloy.[32] As a result, the mechanical toughness of the sintered ingot drastically increases with few percent in volume of the additive constituent, yet at the expense of a decrease of the hardness (Fig. 16). This procedure supplies a way to bypass the intrinsic brittleness of Al-based quasicrystals, which is detrimental to their use in contact mechanics for their reduced friction coefficient (see Section D3 hereafter).

C2 Single grain samples

The physics of CMAs has made tremendous progress during the past decade thanks to the availability of single grain samples of the best structural perfection. We will see in the following that single crystals have now also relevance to potential applications. Different methods may be used to this end, such as Czochralski crystal pulling, or Bridgman growth, or the flux growth method, depending on the ease with which the relevant composition field may be accessed from the liquid region. Fig. 17 shows two beautiful examples of single grain CMAs grown out of Al-rich liquids and the size of which is large enough to allow for measurements of physical properties along the main directions of the crystal.[33]

C3 Surface coatings and thin films

Quasicrystals, and more generally Al-based CMAs, are too brittle to be used in bulk form in many applications. They may

Fig. 17 $Al_4(Cr,Fe)$ (left) and $Al_{13}Co_4$ (right) single grain crystals grown out of Al-rich liquids. Courtesy of P. Gille, University of Munich.

prove useful however as surface coatings or functionalising thin films.[8] Again, various technologies are able to fulfil the goal: thermal spray and plasma spray of atomised powders studied long ago for the first time by the present author,[31] physical vapour deposition (PVD)[34] or more recently set up, chemical vapour deposition.[35] Again, attention must be paid to reach the equilibrium state of the film and avoid trapping it in a metastable state that does not show the properties of interest it is supposed to offer. For example, pre-heating of the substrate, or post-annealing of the coated material is mandatory to obtain a quasicrystalline coating from sprayed Al–Cu–Fe(–Cr) coatings.[31]

Finally, the use of a bond coat will prove advantageous in contact mechanical applications or for reducing adhesion because the coating itself is selected for its low surface energy and therefore offers poor bonding to conventional metallic materials like steel. A solution to this tricky problem is brought when adapting the most complex surface material to the substrate by depositing an intermediate, or bond coat layer made of a CMA of intermediate complexity like the γ-Al_4Cu_9 brass phase.[34,36] Lack of adherence of the CMA surface material to metallic substrates is the principal reason for the failure of the few research programmes aiming at a use of Al-based quasicrystals and CMAs for the reduction of friction. The phenomenon is amplified by the formation of vacancies and nanometric voids at the interface between Al-based CMA and metallic substrate during subsequent annealing in order to reach the stable CMA phase because of the Kirkendall effect provoked by the high difference in diffusion coefficients of Al toward the metallic substrate on the one hand, and metal from the substrate towards the CMA film on the other. Fig. 18 provides an example of an Al–Cu–Fe quasicrystalline thin film obtained by thermal mixing during post-deposition annealing of a multilayer prepared by sequential deposition using PVD of a few Al, Cu and Fe layers matching the sought nominal composition. If the interface of the multilayer to the metallic substrate before annealing is sharp, this is no longer the case after the thermal treatment, which causes embrittlement of the film and later delamination under mechanical contact.[37]

The preparation routes briefly mentioned in this section allow for the production of various types of potentially useful CMAs, including quasicrystals at an industrial production rate.[31] We will distinguish in the following between applications based on transport properties, on mechanical properties, and on chemical properties. This classification is essentially arbitrary because the effect of the different categories of properties is always found mixed in CMAs. For instance,
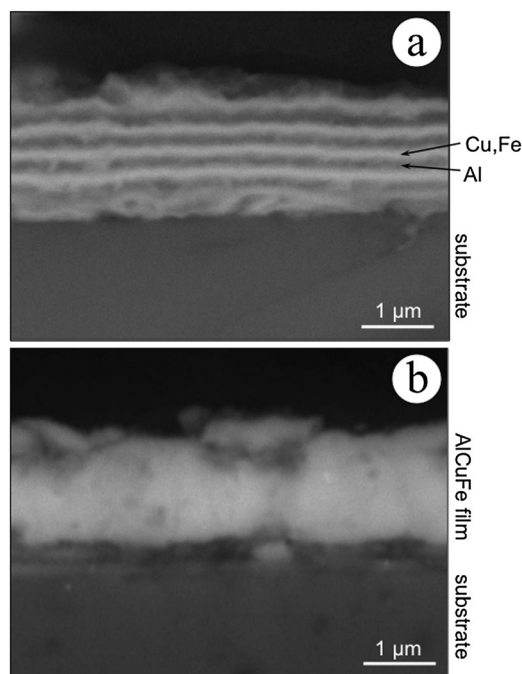
Fig. 18 Preparation of a thin layer of icosahedral AlCuFe on a steel substrate. The preparation starts with the deposition of a multilayer of elemental Al, Cu and Fe layers (a) the thickness of which is monitored to match the nominal composition of the CMA. Thermal mixing by annealing (b) leads to the formation of the icosahedral compound, but is accompanied by the formation of Kirkendall voids at the interface with the substrate. Courtesy of M. Cekada, Jozef Stefan Institute, Ljubljana.

reduction of friction, which is exploiting a mechanical property, is to a large extent due to the low surface energy of highly complex CMAs, which in turn is dominated by the specific electronic structure of those materials. As a consequence, CMA products most often exploit a compromise of otherwise conflicting properties (in standard metallic alloys) and are thus restricted to niche applications.

D Potential applications based on transport properties

D1 Infrared light absorption

The optical conductivity of quasicrystals, in direct relationship to the reduced static conductivity described above, is low and shows no Drude peak at low frequencies in highly perfect aperiodic crystals (Fig. 19), in strong contrast to conventional metals and low complexity CMAs like the γ-brass AlCrFe compound.[38] In multiphased CMA samples, the presence of the Drude peak can be modulated, depending on the phase content of the specimen. In association with the absence of the Drude peak, Al–Cu–Fe quasicrystals exhibit high absorption of infra-red light, with a reflection coefficient as low as $R = 0.6$ at low frequencies, which has to be contrasted to the one found for a good metal like aluminium, which is very close to unity.

This property can be made useful in solar light absorbers like the ones designed by Eisenhammer[39] or the present author
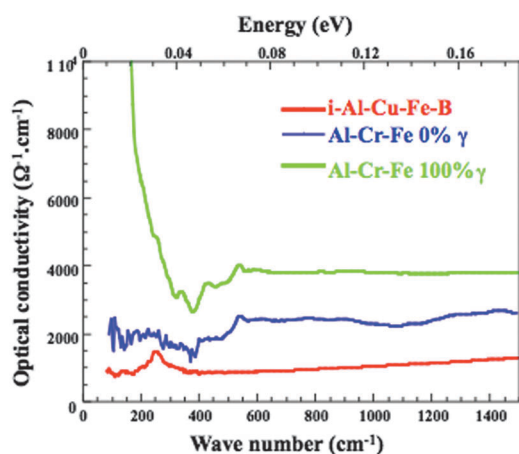
Fig. 19 Optical conductivity measured for sintered, multigrained samples of icosahedral $Al_{59}Cu_{25}Fe_{12}B_3$ (bottom curve) and two Al–Fe–Cr alloys (middle and top curves), one containing only the orthorhombic approximant (noted 0% γ), the other, the γ-brass phase (noted 100% γ).[38]

and his collaborator,[40] with the further advantage over current technologies that the higher thermal stability of quasicrystals may improve the thermodynamic efficiency of the device. Higher costs of production seem however to have prevented commercial exploitation so far.

D2 Reduced adhesion

The present author has pointed out empirically a surprising property of Al–Cu–Fe quasicrystals in the years just following the initial discovery of Shechtman, namely the reduced adhesion of meat towards a surface made of such a material.[41] This experimental evidence can be put on a more rational basis by observing that it is correlated to a lower wetting of a quasicrystal surface by water compared to standard materials like aluminium metal, or its oxide Al_2O_3 (Fig. 20). From this standpoint, the quasicrystal appears as an intermediate between PTFE, a well-known low wetting material, and the native oxide of its main constituent.

A vast research programme was dedicated to setting up the industrial production technology of frying pans utilizing this effect, with the view that it offered an attractive alternative to the Teflon-based technology, presenting much higher resistance against scratch damage thanks to high hardness and much better thermal stability, yet at the expense of a still acceptable, but poorer anti-adhesive behaviour (Fig. 21). The programme unfortunately ended, after the first series of pans were on the market, because the producer decided to skip the mandatory annealing treatment alluded to in the previous section.

The physics behind this phenomenon is still very much an open question, wetting by water and sticking against food being two essentially different questions. The way the author understands the experimentally observed reduction of wetting by water (*i.e.* the increase of the contact angle of a minute droplet of water deposited on that surface compared to the angle measured *e.g.* on pure aluminium) is in direct relationship to the decrease of the R coefficient (previous section) compared to that of Al.[42] The model assumes that the water
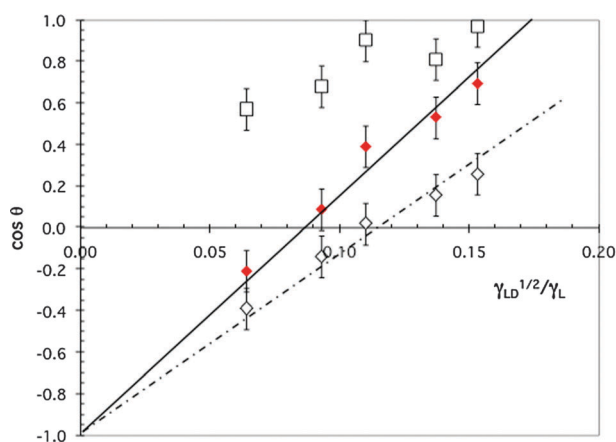

Fig. 20 Variation of the cosine of the contact angle θ of minute droplets of five different liquids deposited on the flat surface of Teflon (open diamonds), alumina (open squares) and a single grain of AlPdMn icosahedral crystal (solid diamonds). The *x*-axis is defined by $x = \sqrt{\gamma_{LW}/\gamma_L}$ with γ_L the surface energy of the liquid and γ_{LW} its Lifshitz–van der Waals component. This plot implies that extrapolation of $\cos\theta$ to $x = 0$ follows a straight line which hits the *y*-axis at -1 if the liquid is non-polar, which is the case for the two liquids located at the highest values of *x*, or if the solid surface itself is non-polar. This is typically the case of Teflon, but obviously not of alumina. Surprisingly, the quasicrystal, although covered by a very thin surface layer of alumina oxide, extrapolates to $\cos\theta = -1$ as a straight line, just like Teflon, but with a larger slope because its own Lifshitz–van der Waals surface component is about twice as large as that of Teflon.[42]

dipoles interact with the electron conduction cloud in the quasicrystal substrate located beneath the native oxide layer always present under ambient conditions *via* the formation of image dipoles within the Fermi sea of electrons. As a consequence, it is expected that the reversible adhesion energy of water on the surface will scale as $n^2(E_F)/t^2$, where t is thickness of the native oxide layer ($t \leq 10$ nm) and $n(E_F)$, the DOS already introduced in this article. Experimental evidence, based upon the study of a large variety of CMAs, with varying DOS at the Fermi energy, equipped with native oxide layers of different thickness t in the range 2–12 nm, is clearly in favour of this model.[42,43] This result suggests that wetting properties (of this specific material) are not only determined by the extreme surface, as would be inferred from current literature on the subject (see articles and books quoted in ref. 42 and 43), but also depend on the internal electronic structure.

D3 Reduced solid friction

Reduction of the friction coefficient of a quasicrystal against a typical indenter like high-Cr hard steel is also a surprising piece of evidence if one compares to hard steel gliding on itself under the same experimental conditions (Fig. 22) since the mechanical properties (hardness, Young modulus, *etc.*) of the two bodies are pretty comparable, but their respective coefficients of friction are different by nearly half an order of magnitude.[43] The pure, very hard alumina oxide also behaves in a totally different way. Unfortunately, the presence of the native oxide layer in ambient air, and tribo-oxidation,[44] added to the intrinsic brittleness already mentioned, limit the hope to see quasicrystals compete with modern self-lubricated low friction materials.
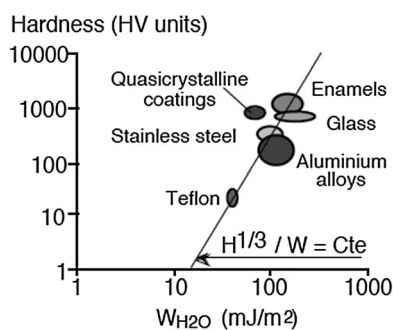
Fig. 21 Pseudo-selection chart presenting quasicrystalline coatings in comparison to other standard materials used for cooking utensils. The selection parameters shown in this figure are the surface hardness, for the ability of the surface to resist scratching, and the reversible adhesion energy of water on that surface (equipped with its native oxide if it is a metallic alloy), for its anti-stick properties. The size of each area is proportional to the scatter of those parameters for each type of material. A correlation seems to manifest itself, but this is only empirical observation. The advantage of quasicrystalline coatings over the other types of materials is a better compromise between hardness and (anti-)adhesion.
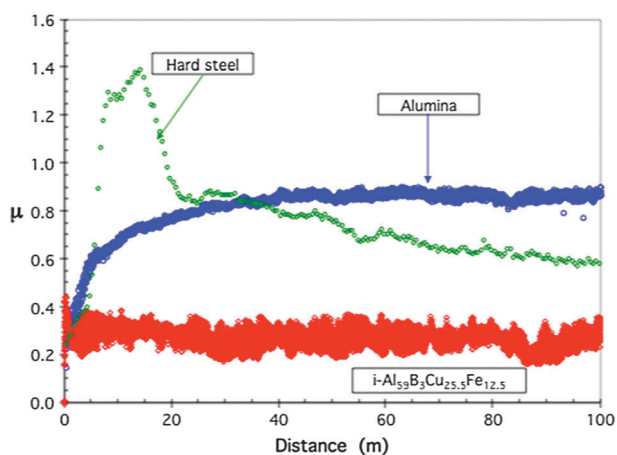
Fig. 22 Friction coefficient measured under secondary vacuum as a function of sliding distance of a hard steel spherical pin gliding on three different disks under a normal load of 2 N and a relative velocity of 5×10^{-2} m s^{-1}. The lowest curve in the figure shows the response of a sintered icosahedral alloy, the one with a peak (due to the emission of wear debris) is for steel riding on itself, and the one that bends smoothly towards the highest friction coefficient is for a multigrained sinter of alumina. Steel is progressively transferred on this sample from indenter to the sliding trace, which means that friction is between steel and itself at the end of the experiment.

In high vacuum technologies (micro-electronics, aerospace, *etc.*), the case is different however and attempts have been produced to prepare non-fretting surfaces that do not stick to each other under mechanical contact and vibrating environment. A typical result of comparative fretting tests under secondary vacuum (the conditions encountered on a satellite) is shown in Fig. 23. A variety of standard metallic alloys (aluminium and Al–Si alloys and a stainless steel) were used under fretting conditions either against themselves (bottom of the figure) or against the Al–Pd–Mn icosahedral quasicrystal or against one of its approximants (top part of the figure).
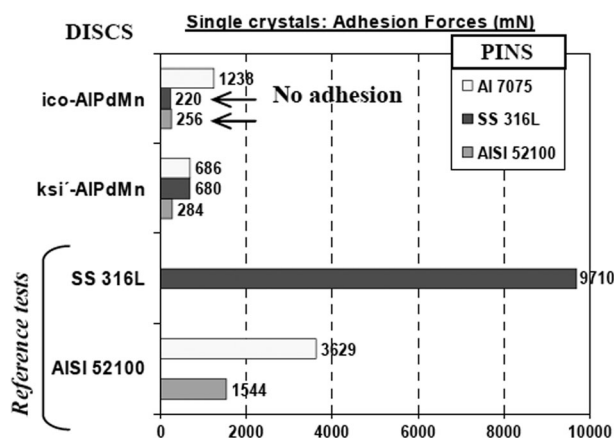
Fig. 23 Stick force evaluated under secondary vacuum by fretting tests applied to two Al–Mn–Pd CMAs (top part of the figure) and two standard materials used in the aeronautic industry (bottom part of the figure). The test consists in loading a spherical pin (inset) under 5 N normal force and move it in contact to the surface under test during typically 100 oscillating runs the amplitude of which is restricted to a few tens of micrometers. The gap between pin and surface is then opened and the adhesion force that resists the opening measured. The process is repeated for thousands of cycles to achieve correct statistical accuracy.

No adhesion is found under the test conditions against these two latter antagonists whereas adhesion, from significant up to huge, is manifest in the case of the conventional alloys.

Fig. 24 illustrates a different usage of the reduced solid–solid adhesion against quasicrystals. Thin films were prepared on sintered tungsten carbide inserts designed for cutting tools, using the technique described in Fig. 18. A standard test was then applied to assess whether the presence of the film increases or not the lifetime of the cutting insert in comparison to the state of the art (standard in Fig. 24). The functional films consisted of three multilayers and two icosahedral PVD coatings. According to the profession, quantitative comparison
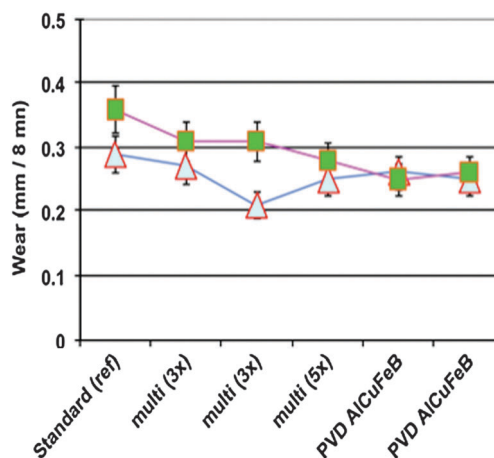
Fig. 24 Results of a wear test applied to WC-Co cutting inserts of the state of the art (noted 'Standard', used as a reference) and covered with three types of Al–Cu–Fe multilayers as shown in Fig. 18 or two different coatings prepared by PVD. The test is standard for the mechanical industry. Its result is given in terms of the broadening due to wear of the cutting edge at two different locations along the edge after a fixed duration of machining.

This journal is © The Royal Society of Chemistry 2012

may be achieved by measuring after a certain time of machining the width of the wear region that forms on the edge of the tool at two different spots along the edge. Quasicrystalline films allow for an increase of the lifetime of the tool by about 25%, which is considered very significant and potentially fruitful by professionals, if the incurred increase of cost of the cutting insert stays low enough, a conclusion that goes beyond the skills of this author.

D4 Heat insulation

A comparison is made in Fig. 25 between the heat conductivity at room temperature typical of a few CMAs and of few conventional materials, including fcc aluminium.[26] Again, as already pointed out earlier in this review, orders of magnitude separate the conductivity of fcc Al and of the Al–Cu–Fe quasicrystal, which falls typically below $\kappa = 1$ W mK^{-1} at RT. Not shown in this figure is the same value of $\kappa = 1$ that characterizes zirconia, a standard insulating material used in aircraft engines to increase their efficiency and prolong the maintenance interval of the turbine blades. A practical use of such a low conductivity is presented in Fig. 26, with the case of a thermal barrier built by magnetron sputtering on the surface of a turbine blade for a helicopter engine. This application takes into account the lower functioning temperature of this type of engine, which fits better to the reduced melting point of this material compared to zirconia, but unfortunately limits its application range. In contrast, expansion coefficients of quasicrystals, that are very similar to the ones of metallic substrates, favour their use since they reduce the interfacial stress generated by thermal cycling between substrate and coating.

D5 Information storage using heat pulses

Dolinsek et al. developed an entirely novel approach to store information bytes without requiring the use of electron transfer,
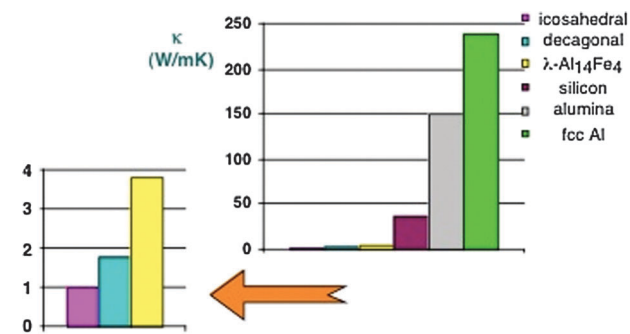

Fig. 25 Room temperature thermal conductivity of a variety of standard materials and of CMAs.

Fig. 26 Small turbine blade covered with a 0.3 mm thick thermal barrier made by magnetron sputtering of an AlCoFeCr CMA (the length of the blade is typically 8 cm). This application fits the needs of helicopter engines, which work at moderate temperatures of the order of 700 °C. Courtesy of S. Drawin, ONERA.

or external magnetic field, or laser light, but only pure thermal manipulation of a magnetically frustrated material, which conveniently can be taken as the Al$_3$(Mn,Fe) CMA or a canonical Cu–Mn spin glass.[45] These are two magnetically frustrated systems that show broken ergodicity below a certain freezing temperature T_f (defined as the cusp easily observable on the magnetization versus temperature curve in the absence of any external field, or zero field curve – zfc). Upon continuous cooling along this zfc curve, the spin system has no time to equilibrate; it freezes in a randomly distributed configuration called a spin glass. The concept of thermal memory cell developed by Dolinsek et al. induces information storage by stopping the continuous cooling at a certain temperature $T_i < T_f$ and leaving the spins that are still mobile at that temperature to equilibrate for a certain time duration of the order of minutes or hours until cooling to lower temperatures continues. The temperature interval between T_f and the lowest accessible temperature can thus be divided into a number of isothermal annealing plateaus, which represent an identical number of information bits, with information bit taken as 1 if the system was stopped to equilibrate at the corresponding temperature, and 0 if no plateau was applied. Storing the material at the lowest temperature keeps the memory of its history, so that it can be read later on by warming up the material in a small external magnetic field to measure its magnetization, which by the way also erases the information.

A thermal memory cell based on a monocrystal of few mm^3 of the T–Al$_3$(Mn,Fe) CMA was used to demonstrate the possibility to encode bytes of 8 bits (i.e. using 8 isothermal plateaus), including storage of ASCII characters** (Fig. 27). The duration of the encoding thermal plateaus was set to 1 hour, which for the time being makes the invention of little practical importance, but Dolinsek et al. stress that the time could be considerably reduced. So far, the thermal memory cell is therefore essentially of fundamental significance.

E Mechanical reinforcement of composites

E1 Metal–matrix composites

Preparation of metal–matrix composites reinforced by quasicrystalline or complex intermetallics has received considerable interest since the beginning of the field. Room is not sufficient in the present review to quote all the published work; the reader may find relevant information in the text books listed in ref. 8. The first, and for a long time only, commercially successful application of quasicrystals was the production of a maraging steel,†† which is hardened by an in situ precipitation of icosahedral nanoparticles.[46] Outstanding mechanical properties result, which allow using this alloy for extremely demanding applications like surgical tools. An international group that produces razors employs it for the fabrication of blades.

** American Standard Code for Information Storage character, which is a 7-bit code for the storage of characters ranked from 0 to 127. In Dolinsek's experiment, the first bit was set to 0 and the 7 other bits used for the ASCII characters.
†† A maraging steel (for martensitic and aging) is a low carbon steel, containing selected additives like Ni, Ta, Mo, etc., that derives its mechanical strength from a precipitation of intermetallics achieved during a specific heat treatment cycle.
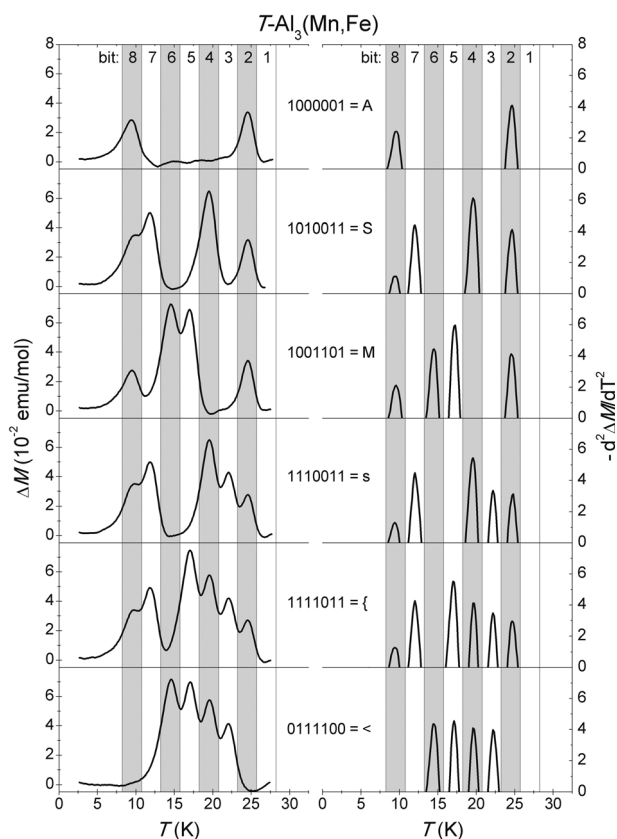
T-Al$_3$(Mn,Fe)

Fig. 27 The TM–Al$_3$(Mn,Fe) thermal memory cell may be used to store ASCII characters with pure thermal manipulations below the freezing temperature of the spin system. Only 7 annealing plateaus were used here to match the ASCII standard, but one more could have been used to store more data. The left hand side column shows the difference in magnetization between a preliminary run made with no annealing steps, used as a baseline (not shown here) and the magnetization recorded upon reading the cell in a small magnetic field. The right hand side column is for the second derivative of the magnetization *vs.* temperature, which shapes properly the signal into 0 and 1 bits.[45] Courtesy of J. Dolinsek, Jozef Stefan Institute, Ljubljana.

In situ precipitation of CMA particles can also be managed during controlled devitrification of metallic glasses, see ref. 8 (Eckert *et al.*) or ref. 47 (Inoue *et al.*). More simply, the metal matrix and the reinforcement particles can be blended using mechanical milling techniques, and later extruded to produce a bulk composite material. Very significant increase of the mechanical performance is then observed in comparison to conventional alloys (Fig. 28 and 29). Fig. 28 shows a bench test of various conventional Al-based alloys compared to three types of extruded materials derived either from atomized icosahedral powders or from initially amorphous atomized powders. The test applies to stress *versus* elongation at rupture observed during tensile test of extruded samples. In Fig. 29, comparison is made of several mechanical properties for the same type of samples *versus* a classical light alloy based on aluminium used in the aeronautics industry. Again, very significant improvement of the mechanical properties is observed.

Phase transformations may occur during annealing treatments managed to consolidate blends of the matrix element
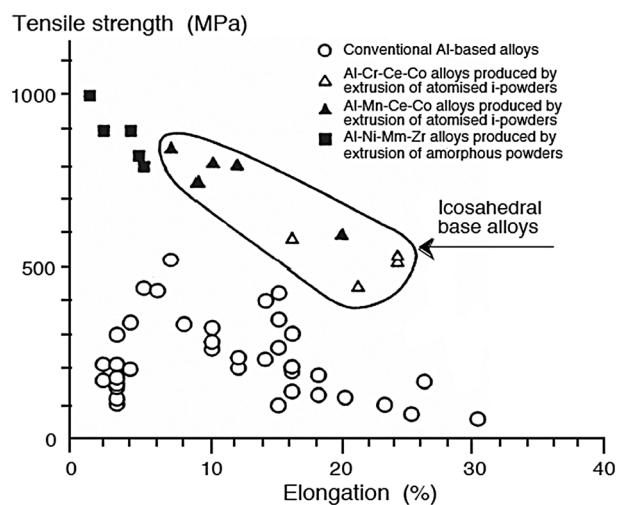
Fig. 28 Tensile strength *versus* elongation at rupture observed for conventional aeronautic aluminium alloys (open dots) and CMA composites prepared by extrusion of atomized icosahedral powders or amorphous powders.[47] Courtesy of A. Inoue, Tohoku University, Sendai.
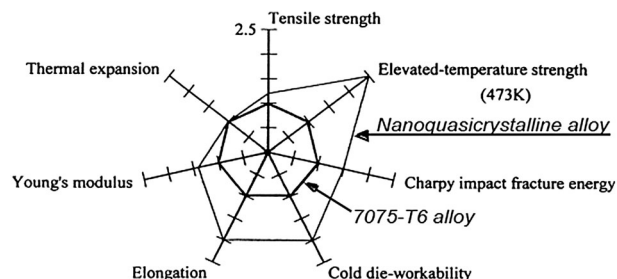

Fig. 29 Benchmark of several mechanical properties characteristic of a high standard light alloy and an extruded nanoquasicrystalline alloy. Courtesy of A. Inoue, Tohoku University, Sendai.

and reinforcing particles produced by mechanical alloying. Tsai *et al.*[48] were the first to observe that mixing aluminium with Al–Cu–Fe icosahedral powders, which indeed increases the hardness of the composite in proportion to the volume of added particles, obeys the phase diagram shown in Fig. 1 and thus leads to the formation of the ω-Al$_7$Cu$_2$Fe phase progressively replacing the icosahedral phase along the duration of the heat treatment. Attempts can be made to preserve the icosahedral phase during heating, for instance by pre-oxidizing the atomized powder in order to place a diffusion barrier at the matrix–particle interface that will block diffusion of aluminium during annealing.[49] The result is however not very spectacular since the barrier is detrimental to the mechanical performance of the composite. In contrast, and surprisingly, composites formed with particles of the ω-phase, either introduced directly as atomized powders, or formed during the annealing process, show quite high mechanical performance regarding yield stress and deformation at rupture (Fig. 30).

### E2 Polymer–matrix composites

Polymer–matrix composites represent another type of material in which quasicrystalline particles, more generally CMA particles, may prove useful as reinforcing media. Very early attempts were
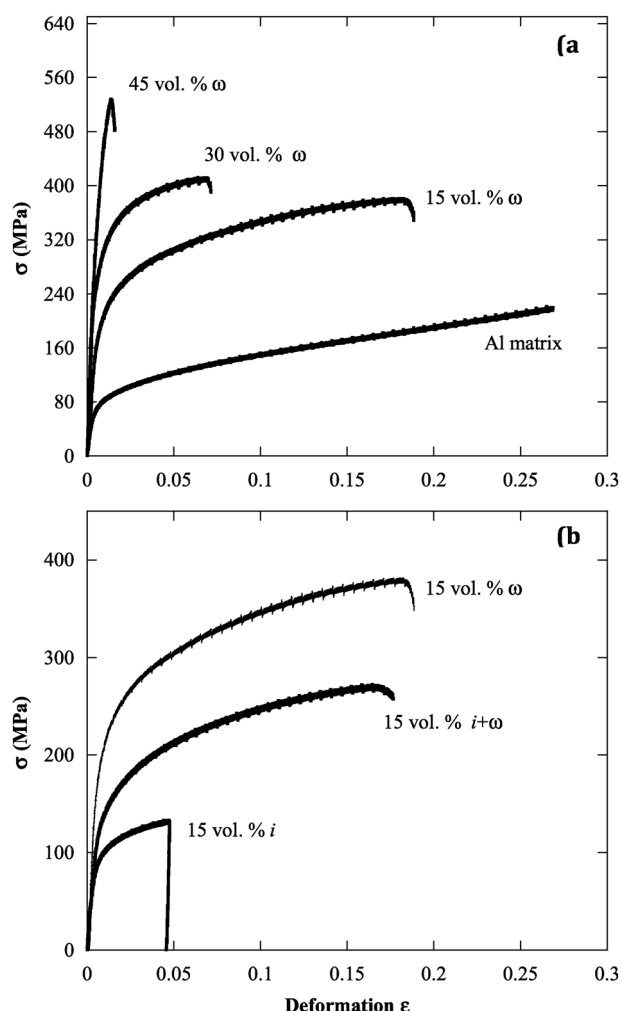
Fig. 30 True stress *versus* true deformation measured in compression of sintered specimens obtained by mixing pure aluminium with the volume fraction indicated in the figure of pre-alloyed ω-Al$_7$Cu$_2$Fe phase (a) and of pure icosahedral powder (bottom curve), partially (middle curve) or totally (top curve) transformed ω-phase formed from initially icosahedral powders after reaction with the aluminium matrix (b).[49]

made by the present author in order to utilize the fraction of small particles, with a diameter below 30–40 μm, that could not be used in the plasma spray technology developed for the production of frying pans (Section D1 above). Independently, Sheares and Bloom proved the beneficial effect of additions (in the range of a few to several tens of weight%) of quasicrystalline powders to quite a variety of different polymers, thus increasing their resistance to abrasion and their mechanical strength.[50] Comparison to other fillers like alumina or silicon carbide particles demonstrated the superiority of quasicrystalline powders, but so far no industrial development followed the invention.

This is not the case for another invention related to the use of atomized, quasicrystalline powders for the reinforcement of a polymer.[51] The context is different; it relates to rapid prototyping of a part in its final shape by selective laser sintering (SLS) of a blend of polymer and filler particles. This technology is now of wide use in many sectors of industry because it allows (i) direct fabrication of net shapes without loss of matter, and (ii) production of complex shapes that could not be machined
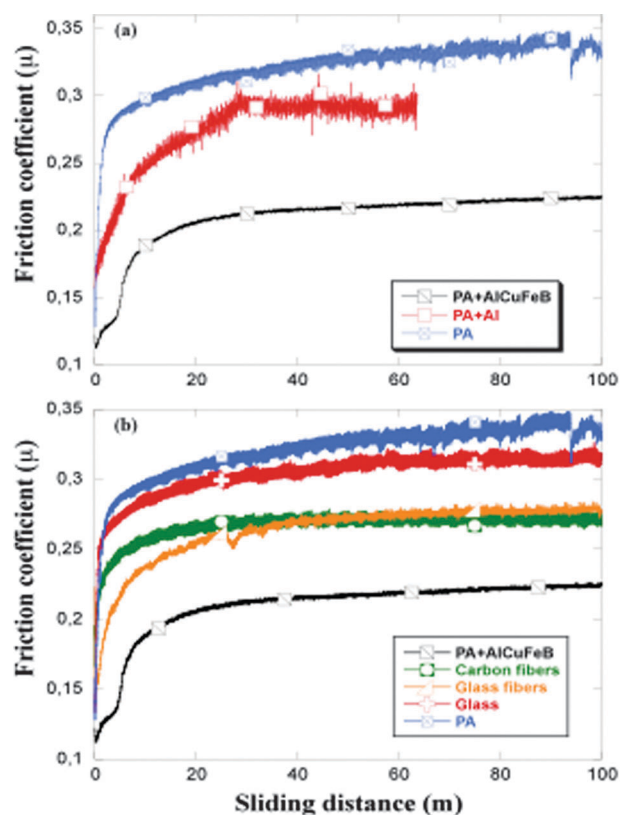
Fig. 31 Pin-on-disk tests supplying the friction coefficient against hard steel as a function of the run distance for (a) polyamide (PA) alone, PA filled with aluminium particles and PA filled with AlCuFeB icosahedral powders and (b) PA reinforced with various fillers as indicated in the inset.[51]

by conventional techniques. SLS is an additive manufacturing process that produces a part in its final shape by locally sintering the polymer when a laser beam hits, layer by layer, the surface of the container in which the powder is placed. Moving the container downwards and replacing the sintered layer by a fresh one allow the manufacture of parts in three dimensions.

The superiority of quasicrystalline powders over conventional fillers like steels is that the grains absorb the laser light (Section D1 above) very efficiently, thus heat up quickly and therefore produce better melting of the surrounding polymer matrix. Adhesion to the filler is then optimized, resulting in no porosity and better mechanical properties, for instance during pin-on-disk tests as shown in Fig. 31. Excellent performance has been achieved from an economical standpoint, to such a level that the powder blend is now available commercially under trademark of a French company. An example of a part manufactured using this process is shown in Fig. 32.

F Potential applications based on chemical properties

F1 Protection against corrosion and oxidation

All studies of quasicrystals and CMAs facing oxidizing or corrosive conditions have shown that their specific crystal structure has virtually no influence on their response to such environments.

Fig. 32 Specific part manufactured by selective laser sintering directly to its final shape, using a blend of polymer and icosahedral AlCuFeB. This part is ready for sale and is an example of a successful, marketed application of quasicrystals.[51]

A summary of a study[52] of the surface composition changes undergone by three Al–Cu–Fe CMAs of quite different complexities, but similar chemical compositions, when placed under different oxidizing conditions is shown in Fig. 33. Starting with the material analysed under ultra-high vacuum, comparison is made for the three constituent elements between the variation observed on the surface concentration after exposure to pure oxygen, to normal air or immersion in water. Although the surface concentration of the three elements moves away from the initial composition in proportion to the strength of the oxidation medium, no significant change is observed between the two more complex alloys. The Al concentration at
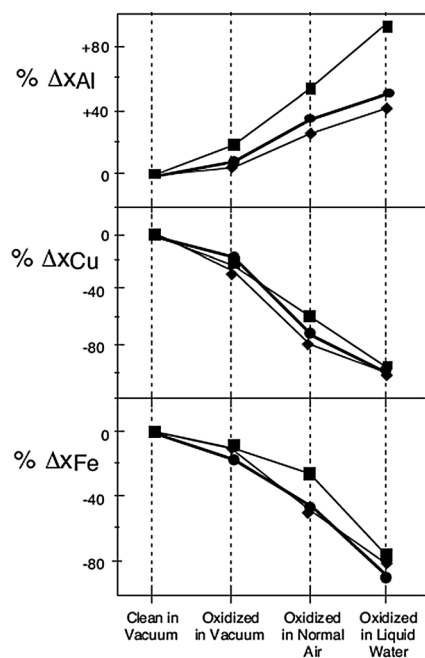
Fig. 33 Change of the surface composition of the three constituent elements of a sample of β-$Al_{51}Cu_{35}Fe_{14}$ (squares), λ-$Al_{75}Cu_3Fe_{22}$ (diamonds) and icosahedral Ψ-$Al_{66}Cu_{22}Fe_{12}$ (dots) when the samples are submitted to the oxidation treatments indicated at the bottom of the figure. Each change is referred to the composition measured on the naked surface under ultra-high vacuum (first column). Redrawn from ref. 52 with permission of P. A. Thiel, Iowa State University.

the surface of the B2-phase is more shifted from the two others after immersion in water, but the same trend is not observed if the experiment is repeated with Al–Pd–Mn CMAs of similar complexities. It is therefore the chemical composition that is beneficial, or not, to a good resistance against corrosive media.

This property orients the selection of certain quasicrystals or CMAs in view of a given application, by choosing among the various compounds that fall in the high-β_C range introduced in a previous section, those which contain elements like Cr or Mo that are known to favour high corrosion resistance in conventional aluminium alloys. The Al–Fe–Cr system is a good candidate for this purpose since it contains a high-order orthorhombic approximant of the decagonal phase (Fig. 2) as well as two varieties of the γ-brass phase.[53] A detailed study[54] of the transformation of the surface of an $Al_{65}Cr_{27}Fe_8$ alloy that was abandoned in ambient air for long durations proved that the surface progressively consists of a stacking of layers of amorphous oxides of the constituents onto which a layer of hydroxide builds up as well as a contamination layer (Fig. 34). The same behaviour is typically observed on other metallic alloys containing chromium, and characterizes an appreciable resistance to aging, under such conditions. The manufacture of frying pans was directly dependent upon the possibility to reduce drastically the emission of Al and other elemental constituents during cooking, including in pretty drastic corrosive media like vinegar with sodium chloride that are currently used in cooking.[31] Many more details about the surface chemistry of quasicrystals and CMAs may be found in the text books quoted under ref. 8.

F2 Hydrogen storage

The Ti–Ni–Zr system yields a metastable quasicrystal and an approximant at very closely related compositions.[6] Both are capable of hydrogen loading, the quasicrystal showing higher hydrogen content after cycling under H_2 pressure (Fig. 35). They both transform upon heating into more stable configurations. This observation has led to several assessment studies of the hydrogen capacity that could be stored into the more efficient quasicrystal. No superiority towards more conventional materials could be demonstrated however, due to the diffusion barrier formed by the native surface oxide and metallurgical difficulties in processing this material that is very reactive against oxygen.

The case was revisited recently by Kocjan et al. who pointed out a surprisingly interesting conclusion.[55] Melt-spun ribbons
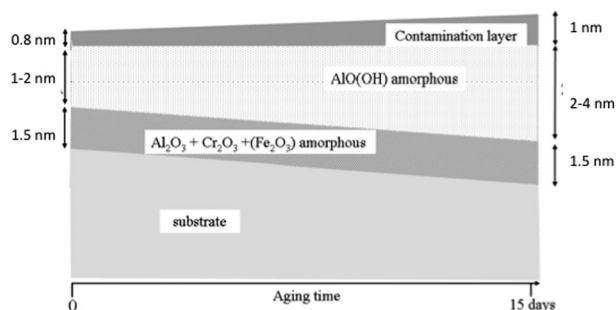
Fig. 34 Model of the evolution of the surface layer structure of an $Al_{65}Cr_{27}Fe_8$ alloy left in ambient air for two weeks.[54]
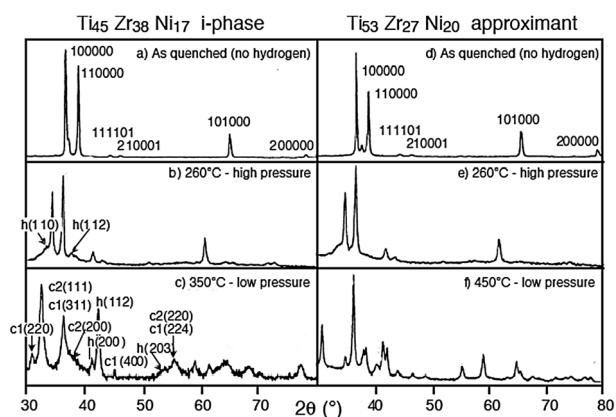
Fig. 35 X-ray diffraction patterns (λ = KαCu) of Ti–Zr–Ni samples, one icosahedral (left), the other approximant (right) before (top row) and after H$_2$ loading (middle and bottom rows) at two different temperatures as indicated. Redrawn from ref. 6 with permission of K. Kelton, Washington University in St Louis.
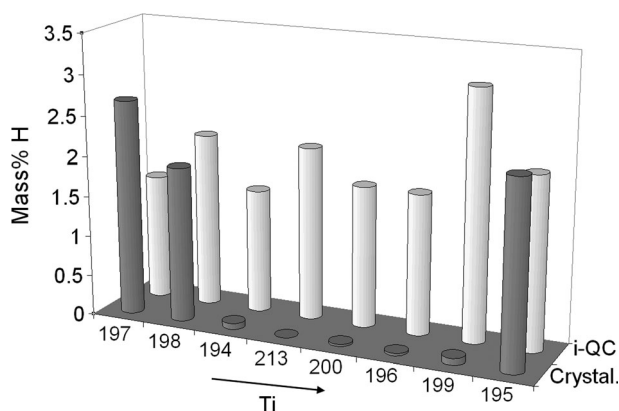
Fig. 36 Mass change upon H$_2$ loading of crystalline (front row) and icosahedral (back row) Ti–Zr–Ni alloys at constant Ni content and variable Ti/Zr ratio (numbers label the different samples used in the study).[55] Courtesy of S. Kobe, Jozef Stefan Institute, Ljubljana.

were prepared at constant Ni concentration and varying Ti/Zr ratio in the Ti–Ni–Zr system, which resulted in metastable quasicrystals as already mentioned, from which stable crystals could be prepared by high temperature annealing. Upon loading with hydrogen, a region was found in the phase diagram in which the crystals load no hydrogen whereas the quasicrystals do load significant amounts of hydrogen. No difference was found between the two lattice types outside that region (Fig. 36). This result is interesting because, in contrast to corrosion resistance, chemistry does not matter, but instead the crystal structure, whether it is periodic or not. The authors of ref. 55 emphasize that the surface oxide is much thicker on the crystals than on the quasicrystals, but other phenomena like phason flips‡‡ may also play a role and distinguish between the two crystal states. Whether this study[55] will re-launch the quest for a new hydrogen storing material is still an open question.

‡‡ Phason flips are atomic movements specific to quasicrystals. See the article dedicated to high dimensional crystallography in this special issue.
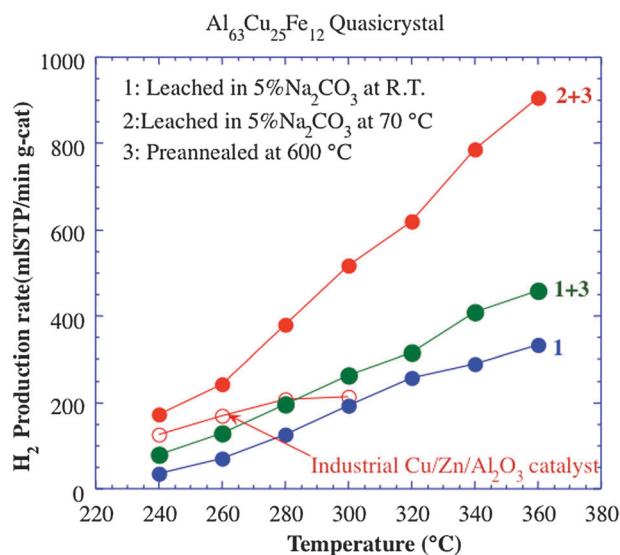
Fig. 37 Production rate of hydrogen during methanol reforming using AlCuFe icosahedral powders leached under the conditions indicated in the figure, in comparison to the rate observed with a standard, industrial catalyst (open circles).[56] Courtesy of A. P. Tsai, NIRIM, Sendai.

F3 Catalysis

Catalysis was placed at the heart of quasicrystal research when Tsai and his co-workers[56] prepared ultra-fine Cu particles by leaching bulk Al–Cu–Fe quasicrystalline alloys in an alkaline solution (Fig. 37). These particles exhibit catalytic activity that competes with the activity of commercial catalysts, thus offering a way to save on the usually costly materials used in the chemical industry. A comparative example is given in Fig. 37 for the case of icosahedral Al$_{63}$Cu$_{25}$Fe$_{12}$ leached under different conditions *versus* an industrial catalyst used for the production of H$_2$ from methanol reforming reaction. Other precursors like the Al–Pd–Mn quasicrystal may be used as well. All show high efficiency and selectivity, to such an extent that they may now
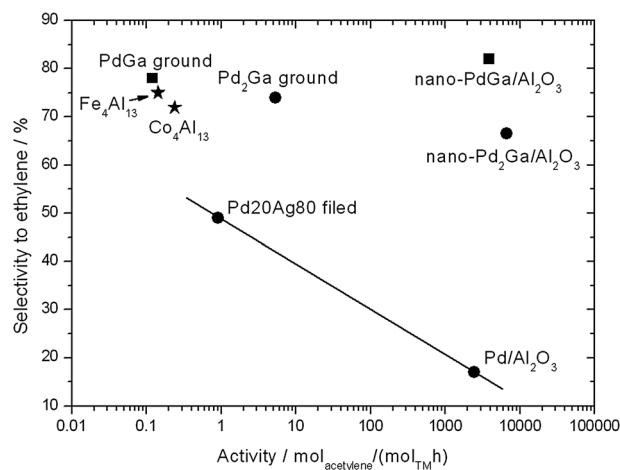
Fig. 38 Selectivity *versus* activity observed during the semi-oxidation reaction of acetylene with different catalysts as indicated in the figure, including the standard Pd/Al$_2$O$_3$ catalyst used in industry.[57] The two CMAs discussed in text are represented by stars. Courtesy of M. Armbruster, Max Planck Inst. for Chemical Physics of Solids, Dresden.

be considered as good candidates for the replacement of older, more expensive catalysts like Pd and Pd.

Specific configurations existing at the surface of naked CMAs also show high catalytic activity as was pointed out first by Ambruster et al.[57] An example is the semi-hydrogenation of acetylene for which the $Al_{13}Co_4$ and $Al_{13}Fe_4$ decagonal approximants demonstrate high activity, and simultaneously high selectivity, which are far superior to the state of the art and comparable to new generation catalysts (Fig. 38). This discovery has an enormous potential for economic impact on the chemical industry. It has justified so far many theoretical and experimental studies to understand better which surface configurations are responsible for the catalytic behaviour, the description of which goes beyond the scope of this review, see e.g. Addou et al.[58]

G Conclusions: dreams, achievements, and the route to Stockholm

The list of applications of quasicrystals and their parent crystals given in this review is for sure not complete, although the author is convinced that his account is fair for the time being. Very few dreams of application have reached the standard of commercialisation. One such attempt, despite quasicrystal-based products had been put on the market, has failed later on because the mandatory heat treatment was skipped by the producer, thus inducing lack of corrosion resistance and inadequate surface properties. Few more are still in their infancy; competition with products already on the market may forbid any marketing in future, as is often the case with innovative products, or just opposite, may favour their commercialisation because the new product brings unsuspected advantages or solves some drawback of existing materials. This is e.g. the claim made in a recent note[59] that time has come now for quasicrystals in frying pans to replace Teflon® the use of which will soon be forbidden for cooking food in the United States.

Based on the reasonable potential for applications foreseen from the many results available in the 1990's, several important research programmes have been undertaken, in France first, then in the US and Japan, later in China, India, Europe, Brazil, etc. They represent a very significant investment in both human resources and funding that has undoubtedly contributed to the development of the field of quasicrystals research. Most properties discussed in this review could not be anticipated from the knowledge of the composition and that of the metallurgy of conventional Al-based alloys. Having pointed out so many unforeseen applicable properties means that the impact of the discovery of quasicrystals goes far beyond a change of paradigm in crystallography and a better understanding of the way ancient painters decorated Mosques in the Middle East or in Spain (citation of the 2011 Nobel Prize in Chemistry). That the change of paradigm was key in the advancement of solid state sciences cannot be doubted, nor that it deserved a long awaited award in Stockholm. The existence of a deep pseudo-gap at the Fermi level, the near insulator behaviour in electron conduction or heat transfer, the high absorption rate of infra-red light, the reduced friction coefficient against the materials tested so far, the correlated

anti-stick properties, etc. were alluded to during the official presentation of the prize (http://www.nobelprize.org/nobel_prizes/chemistry/laureates/2011/announcement.html). It was more than a delightful surprise to the present author who dedicated two and a half decades of his professional life to the field.[60] This surprise reinforced his pride to have in a way or the other contributed to the progress of this new discipline in condensed matter physics and chemistry, and his happiness to see, so many years after the seminal PRL article,[1] the Nobel Prize in Chemistry recognise in 2011 the fantastic discovery of Daniel Shechtman.

Acknowledgements

Notes and references

1 D. Shechtman, I. Blech, D. Gratias and J. W. Cahn, Phys. Rev. Lett., 1984, 53(20), 1951.
2 A. P. Tsai, A. Inoue and T. Masumoto, Jpn. J. Appl. Phys., 1987, 26, 1505.
3 A. P. Tsai, A. Inoue and T. Masumoto, Mater. Trans., JIM, 1989, 30, 463.
4 A. J. Bradley and H. J. Goldschmidt, J. Inst. Met., 1939, 62, 389–403.
5 A. P. Tsai, J. Q. Guo, E. Abe, H. Takakura and T. J. Sato, Nature, 2000, 408, 537.
6 A. M. Viano, R. M. Stroud, P. C. Gibbons, A. F. McDowell, M. S. Conradi and K. F. Kelton, Phys. Rev. B: Condens. Matter Mater. Phys., 1995, 51(17), 12026.
7 B. Dubost, J. M. Lang, M. Tanaka, P. Sainfort and M. Audier, Nature, 1986, 324, 48.
8 J. M. Dubois, Useful Quasicrystals, World Scientific, Singapore, 2005; Book Series on Complex Metallic Alloys, ed. E. Belin-Ferré, World Scientific, Singapore, 2007–2010, vol. 1–4; Complex Metallic Alloys, Fundamentals and Applications, ed. J. M. Dubois and E. Belin-Ferré, Wiley, Weinheim, 2011.
9 M. Quiquandon, A. Quivy, J. Devaud, F. Faudot, S. Lefebvre, M. Bessière and Y. Calvayrac, J. Phys.: Condens. Matter, 1996, 8, 2487.
10 M. Quiquandon, A. Quivy, J. Devaud, F. Faudot, S. Lefebvre, M. Bessière and Y. Calvayrac, J. Phys.: Condens. Matter, 1996, 8, 2487; A. Quivy, M. Quiquandon, Y. Calvayrac, F. Faudot, D. Gratias, C. Berger, R. A. Brand, V. Simonet and F. Hippert, J. Phys.: Condens. Matter, 1996, 8, 4223.
11 C. Janot, Quasicrystals, a Primer, Oxford Sci. Pub., Oxford, 1994.
12 Y. Lei, S. Kenzari, V. Demange, V. Fournée and J. M. Dubois, Philos. Mag. Lett., 2008, 88(4), 279.
13 C. Dong, J. M. Dubois, S. S. Kang and M. Audier, Philos. Mag. B, 1992, 65(1), 107; S. S. Kang, B. Malaman, G. Venturini and J. M. Dubois, Acta Crystallogr., Sect. B: Struct. Sci., 1992, 48, 770.
14 L. Behara, M. Duneau, H. Klein and M. Audier, Philos. Mag. A, 1997, 76, 587.
15 P. A. Bancel and P. A. Heiney, Phys. Rev. B: Condens. Matter Mater. Phys., 1986, 33, 7917; J. Friedel and F. Denoyer, C. R. Acad. Sci., Paris Ser. IIc: Chim., 1987, 305, 171.
16 W. Hume-Rothery, J. Inst. Met., 1926, 35, 295.

17 U. Mizutani, *Hume-Rothery Rules for Structurally Complex Alloy Phases*, CRC Press, Boca Raton, 2011.

18 D. Mayou, F. Cyrot-Lackmann and G. Trambly de Laissardière, *et al.*, *J. Non-Cryst. Solids*, 1993, **153–154**, 412.

19 M. Feuerbacher, *et al.*, *Z. Kristallogr.*, 2007, **222**, 259.

20 E. Belin-Ferré and J. M. Dubois, *Philos. Mag.*, 2008, **88**, 2163.

21 E. Belin-Ferré, *J. Phys.: Condens. Matter*, 2002, **14**, R1.

22 U. Mizutani, *J. Phys.: Condens. Matter*, 1998, **10**, 4609.

23 N. F. Mott, *J. Non-Cryst. Solids*, 1968, **1**, 1; , *Philos. Mag.*, 1969, **19**, 835.

24 E. Belin-Ferré, V. Fournée and J. M. Dubois, *J. Phys.: Condens. Matter*, 2000, **12–37**, 8159.

25 E. Belin-Ferré, M. Klanjsek, Z. Jaglicic, J. Dolinsek and J. M. Dubois, *J. Phys.: Condens. Matter*, 2005, **17**, 6911.

26 J. M. Dubois, S. S. Kang, P. Archambault and B. Colleret, *J. Mater. Res.*, 1993, **8**(1), 38; A. Perrot and J. M. Dubois, *Ann. Chim. Fr., Special Issue on Quasicrystals*, 1993, **18**, 501.

27 J. Dolinsek and A. Smontara, in *Complex Metallic Alloys, Fundamentals and Applications*, ed. J. M. Dubois and E. Belin-Ferré, Wiley, Weinheim, 2011.

28 P. Bak, *How Nature Works: the Science of Self-Organized Criticality*, 1996, Copernicus Press, New York, NY.

29 J. M. Dubois and P. Weinland, *French Patent* n° 8810559, 1988 & PCT n° FR89/00403, 1989; J. M. Dubois and A. Pianelli, *French Patent* n°2671808, 1991 & PCT n° FR92/00030, 1992.

30 S. Kenzari, D. Bonina, J. M. Dubois and V. Fournée, *Scr. Mater.*, 2008, **59**, 583.

31 J. M. Dubois, A. Proner, B. Bucaille, Ph. Cathonnet, C. Dong, V. Richard, A. Pianelle, Y. Massiani, S. Ait-Yaazza and E. Belin-Ferré, *Ann. Chim. Fr.*, 1994, **19**, 3.

32 D. Cavalcante-Guedes de Lima, *PhD thesis report*, Universitad Federal de Paraïba, Brazil, 2011, unpublished.

33 J. Dolinšek, *Chem. Soc. Rev.*, 2012, **41**, DOI: 10.1039/C2CS35036J, this special issue.

34 T. Duguet, V. Fournée, J. M. Dubois and T. Belmonte, *Surf. Coat. Technol.*, 2010, **205**, 9.

35 L. Aloui, T. Duguet, F. Haidara, M.-C. Record, D. Samélor, F. Senocq, D. Mangelinck and C. Vahlas, *Appl. Surf. Sci.*, DOI: 10.1016/j.apsusc.2012.03.053, in press.

36 T. Duguet, J. Ledieu, J. M. Dubois and V. Fournée, *J. Phys.: Condens. Matter*, 2008, **20**, 314009.

37 S. Polishchuk, P. Boulet, A. Mézin, M.-C. de Weerd, S. Weber, J. Ledieu, J. M. Dubois and V. Fournée, *J. Mater. Res.*, 2012, **27–5**, 837.

38 V. Demange, A. Milandri, M.-C. de Weerd, F. Machizaud, G. Jeandel and J. M. Dubois, *Phys. Rev. B: Condens. Matter Mater. Phys.*, 2002, **6–14**, 144205.

39 T. Eisenhammer and M. Lazarov, *German Patent* n° 4425140, 1994; T. Eisenhammer, *Thin Solid Films*, 1995, **270**, 1.

40 F. Machizaud and J. M. Dubois, *French Patent*, n° 95.03939, 1995.

41 J. M. Dubois, S. S. Kang and Y. Massiani, *J. Non-Cryst. Solids*, 1993, **153–154**, 443.

42 J. M. Dubois, *J. Non-Cryst. Solids*, 2004, **334–335**, 481.

43 E. Belin-Ferré and J. M. Dubois, *Int. J. Mater. Res.*, 2006, **97**, 7.

44 I. L. Singer, J. M. Dubois, J. M. Soro, D. Rouxel and J. von Stebut, in *Quasicrystals*, ed. S. Takeuchi and T. Fujiwara, World Scientific, Singapore, 1998, p. 769.

45 J. Dolinsek, M. Feuerbacher, M. Jagodič, Z. Jagličić, M. Heggen and K. Urban, *J. Appl. Phys.*, 2009, **106**, 043917.

46 A. H. Stigenberg, J. O. Nilsson and P. Liu, *Swedish Patent Appl.* 9303280, 1993; P. Liu, A. P. Stigenberg and J. O. Nilsson, *Scr. Metall. Mater.*, 1994, **31**, 249.

47 A. Inoue and H. M. Kimura, in *Quasicrystals: Preparation, Properties and Applications*, ed. J. M. Dubois, P. A. Thiel, A. P. Tsai and K. Urban, Mat. Res. Soc., Warrendale, 1999, p. 495.

48 A. P. Tsai, K. Aoki, A. Inoue and T. Masumoto, *J. Mater. Res.*, 1993, **8**, 5.

49 S. Kenzari, P. Weisbecker, M. Curulla, G. Geandier, V. Fournée and J. M. Dubois, *Philos. Mag.*, 2008, **88**(5), 755.

50 V. Sheares and P. Bloom, *Intern. Patent* n° WO 00/56538, 2000, Sept. 28.

51 S. Kenzari and V. Fournée, *French Patent*, n° FR2950826, 2009, PCT n° WO2011/039469, 2010; S. Kenzari, D. Bonina, J. M. Dubois and V. Fournée, *Mater. Design*, 2012, **35**, 691.

52 P. J. Pinhero, D. J. Sordelet, J. W. Anderegg, P. Brunet, J. M. Dubois and P. A. Thiel, in *Quasicrystals, Preparation, Properties and Applications*, ed. J. M. Dubois, P. A. Thiel, A. P. Tsai and K. Urban, Materials Research Society, Warrendale, 1999, p. 263.

53 V. Demange, J. Ghanbaja, F. Machizaud and J. M. Dubois, *Philos. Mag.*, 2005, **85**(12), 1261.

54 D. Veys, P. Weisbecker, B. Domenichini, S. Weber, V. Fournée and J. M. Dubois, *J. Phys.: Condens. Matter*, 2007, **19**, 376207.

55 A. Kocjan, S. Kovačič, A. Gradišek, P. J. McGuiness, T. Apih, J. Dolinšek and S. Kobe, *Int. J. Hydrogen Energy*, 2011, **36**(4), 3056.

56 S. Kameoka, T. Tanabe and A. P. Tsai, *Catal. Today*, 2004, **93–95**, 23.

57 M. Ambruster, Y. Grin, K. Kovnir and R. Schlögel, in *Complex Metallic Alloys, Fundamentals and Application*, ed. J. M. Dubois and E. Belin-Ferré, Wiley, Weinheim, 2011.

58 R. Addou, E. Gaudry, Th. Deniozou, M. Heggen, M. Feuerbacher, P. Gille, Y. Grin, R. Widmer, O. Gröning, V. Fournée, J. M. Dubois and J. Ledieu, *Phys. Rev. B: Condens. Matter Mater. Phys.*, 2009, **80**, 014203.

59 MRS Bull., *News and Analysis*, 2011, **36**, 581.

60 J. M. Dubois, *Isr. J. Chem.*, 2011, **51**, 1168.